Supercontinuum generation and soliton timing jitter in SF6 soft glass photonic crystal fibers

Anatoly Efimov and Antoinette J. Taylor

Center for Integrated Nanotechnologies, Materials Physics and Applications, Los Alamos National Laboratory, Los Alamos, NM 87544

efimov@lanl.gov

Abstract: We use broadband frequency-resolved optical gating (FROG) and cross-correlation FROG (XFROG) techniques to study the details of the supercontinuum generated in extruded soft glass SF6 photonic crystal fibers pumped with envelope-modulated 100 fs pulses at telecom wavelengths. Strong temporal jitter of solitons is observed with highly non-Gaussian statistics, which is related to the statistics of the pump pulse envelope shape fluctuations. The ripples present on the input pulse seed the modulation instability at high pump powers, affecting soliton fission. Numerical modeling confirms strong sensitivity of the soliton fission process to the presence of ripples on the pump pulse envelope.

OCIS codes: (060.5530) Pulse propagation and temporal solitons; (060.7140) Ultrafast processes in fibers, (320.6629) Supercontinuum generation.

References and links

1. D. von der Linde,"Characterization of the noise in continuously operating mode-locked lasers," Appl. Phys. B **39,** 201–217 (1986).
2. M. Nakazawa, K. Tamura, H. Kubota, and E. Yoshida, "Coherence Degradation in the Process of Supercontinuum Generation in an Optical Fiber," Opt. Fiber Technol. **4,** 215–223 (1998).
3. M. Bellini, T. W. Hänsch, "Phase-locked white-light continuum pulses: toward a universal optical frequency-comb synthesizer," Opt. Lett. **25,** 1049–1051 (2000).
4. T. M. Fortier, J. Ye, and S. T. Cundiff, "Nonlinear phase noise generated in air-silica microstructure fiber and its effect on carrier-envelope phase," Opt. Lett. **27,** 445–447 (2002).
5. K. L. Corwin, N. R. Newbury, J. M. Dudley, S. Coen, S. A. Diddams, B. R. Washburn, K. Weber, R. S. Windeler, "Fundamental amplitude noise limitations to supercontinuum spectra generated in a microstructured fiber," Appl. Phys. B **77,** 269–277 (2003).
6. J. N. Ames, S. Ghosh, R. S. Windeler, A. L. Gaeta, S. T. Cundiff, "Excess noise generation during spectral broadening in a microstructured fiber," Appl. Phys. B **77,** 279–284 (2003).
7. N. R. Newbury, B. R. Washburn, K. L. Corwin, R. S. Windeler, "Noise amplification during supercontinuum generation in microstructure fiber," Opt. Lett. **28,** 944–946 (2003).
8. X. Gu, M. Kimmel, A. P. Shreenath, R. Trebino, J. M. Dudley, S. Coen, R. S. Windeler, "Experimental studies of the coherence of microstructure-fiber supercontinuum," Opt. Express **11,** 2697–2703 (2003).
9. F. Lu and W. H. Knox, "Generation of a broadband continuum with high spectral coherence in tapered single-mode optical fibers," Opt. Express **12,** 347–353 (2004).
10. S. M. Kobtsev, S. V. Kukarin, N. V. Fateev, S. V. Smirnov, "Coherent, polarization and temporal properties of self-frequency shifted solitons generated in polarization-maintaining microstructured fibre," Appl. Phys. B **81,** 265–269 (2005).
11. I. Zeylikovich, V. Kartazaev, and R. R. Alfano, "Spectral, temporal, and coherence properties of supercontinuum generation in microstructure fiber," J. Opt. Soc. Am. B **22,** 1453–1460 (2005).
12. D. R. Solli, C. Ropers, P. Koonath, and B. Jalali, "Optical rogue waves," Nature (London) **450,** 1054–1058 (2007).

#93705 - $15.00 USD Received 12 Mar 2008; revised 9 Apr 2008; accepted 9 Apr 2008; published 11 Apr 2008

13. J. M. Dudley, G. Genty, and B. J. Eggleton "Harnessing and control of optical rogue waves in supercontinuum generation," Opt. Express **16,** 3644–3651 (2008).
14. G. P. Agrawal, *Nonlinear Fiber Optics*, (Academic Press, San Diego, 2001).
15. J. M. Dudley, G. Genty, S. Coen, "Supercontinuum generation in photonic crystal fiber," Rev. Mod. Phys. **78,** 1135–1184 (2006).
16. M. N. Islam, G. Sucha, I. Bar-Joseph, M. Wegener, J. P. Gordon, and D. S. Chemla, "Broad bandwidths from frequency-shifting solitons in fibers," Opt. Lett. **14,** 370–372 (1989).
17. M. N. Islam, G. Sucha, I. Bar-Joseph, M. Wegener, J. P. Gordon, and D. S. Chemla, "Femtosecond distributed soliton spectrum in fibers," J. Opt. Soc. Am. B **6** 1149–1158 (1989).
18. J. M. Dudley, L. P. Barry, P. G. Bollond, J. D. Harvey, R. Leonhardt, "Characterizing Pulse Propagation in Optical Fibers around 1550 nm Using Frequency-Resolved Optical Gating," Opt. Fiber Technol. **4,** 237–265 (1998).
19. F. G. Omenetto, B. P. Luce, D. Yarotski, A. J. Taylor, "Observation of chirped soliton dynamics at $\lambda = 1.55\ \mu$m in a single-mode optical fiber with frequency-resolved optical gating," Opt. Lett. **24,** 1392–1394 (1999).
20. X. Gu, L. Xu, M. Kimmel, E. Zeek, P. O'Shea, A. P. Shreenath, and R. Trebino, "Frequency-resolved optical gating and single-shot spectral measurements reveal fine structure in microstructure-fiber continuum," Opt. Lett. **27,** 1174–1176 (2002).
21. J. M. Dudley, X. Gu, L. Xu, M. Kimmel, E. Zeek, P. O'Shea, R. Trebino, S. Coen, R. S. Windeler, "Cross-correlation frequency resolved optical gating analysis of broadband continuum generation in photonic crystal fiber: simulations and experiments," Opt. Express **10,** 1215–1221 (2002).
22. T. Hori, N. Nishizawa, T. Goto, M. Yoshida, "Experimental and numerical analysis of widely broadened supercontinuum generation in highly nonlinear dispersion-shifted fiber with a femtosecond pulse," J. Opt. Soc. Am. B **21** 1969–1980 (2004).
23. S. N. Bagayev, V. I. Denisov, V. F. Zakhar'yash, V. M. Klement'ev, S. M. Kobtsev, I. I. Korel', S. A. Kuznetsov, S. V. Kukarin, V. S. Pivtsov, S. V. Smirnov, N. V. Fateev, "Spectral and temporal characteristics of a supercontinuum in tapered optical fibres," Quantum Electron. **34** 1107–1115 (2004).
24. S. O. Konorov, D. A. Akimov, A. A. Ivanov, E. E. Serebryannikov, M. V. Alfimov, K. V. Dukelskii, A. V. Khokhlov, V. S. Shevandin, Yu. N. Kondratev, A. M. Zheltikov, "Spectrally and temporally isolated Raman soliton features in microstructure fibers visualized by cross-correlation frequency-resolved optical gating," Appl. Phys. B **79** 289–292 (2004).
25. V. V. Ravi Kanth Kumar, A. K. George, W. H. Reeves, J. C. Knight, P. St. J. Russell, "Extruded soft glass photonic crystal fiber for ultrabroad supercontinuum generation," Opt. Express **10** 1520–1525 (2002).
26. A. Efimov, A. J. Taylor, "Cross-correlation frequency-resolved optical gating for studying ultrashort-pulse nonlinear dynamics in arbitrary fibers," Appl. Opt. **44** 4408–4411 (2005).
27. D. V. Skryabin, and A. V. Yulin, "Theory of generation of new frequencies by mixing of solitons and dispersive waves in optical fibers," Phys. Rev. E **72,** 016619 (2005).
28. F. G. Omenetto, N. A. Wolchover, M. R. Wehner, M. Ross, A. Efimov, A. J. Taylor, V. V. R. K. Kumar, A. K. George, J. C. Knight, N. Y. Joly, P. St. J. Russell, "Spectrally smooth supercontinuum from 350 nm to 3 μm in sub-centimeter lengths of soft-glass photonic crystal fibers," Opt. Express **14,** 4928–4934 (2006).
29. A. Efimov, A. V. Yulin, D. V. Skryabin, J. C. Knight, N. Joly, F. G. Omenetto, A. J. Taylor, and P. St. J. Russell, "Interaction of an Optical Soliton with a Dispersive Wave," Phys. Rev. Lett. **95,** 213902 (2005).
30. A. Efimov, A. J. Taylor, A. V. Yulin, D. V. Skryabin, and J. C. Knight, Opt. Lett. **31,** 1624–1626 (2006).
31. A. Efimov, A. J. Taylor, F. G. Omenetto, A. V. Yulin, N. Y. Joly, F. Biancalana, D. V. Skryabin, J. C. Knight, P. St. J. Russell, "Time-spectrally-resolved ultrafast nonlinear dynamics in small-core photonic crystal fibers: Experiment and modelling," Opt. Express **12,** 6498–6507 (2004).
32. A. V. Gorbach, D. V. Skryabin, J. M. Stone, J. C. Knight, "Four-wave mixing of solitons with radiation and quasi-nondispersive wave packets at the short-wavelength edge of a supercontinuum," Opt. Express **14,** 9854–9863 (2006).
33. A. Podlipensky, P. Szarniak, N. Y. Joly, C. G. Poulton, and P. St. J. Russell, "Bound soliton pairs in photonic crystal fiber," Opt. Express **15,** 1653–1662 (2007).
34. A. Efimov, A. J. Taylor, F. G. Omenetto, E. Vanin, "Adaptive control of femtosecond soliton self-frequency shift in fibers," Opt. Lett. **29,** 271–273 (2004).

1. Introduction

Coherence properties of supercontinua (SC) generated with nonlinear methods are important for most of the practical applications. A number of approaches exist to measure both phase and amplitude fluctuations as a function of wavelength [1–11], however, typically the statistics of the noise is not determined. Only recently, the statistical properties of the fluctuating SC attracted attention of the research community [12, 13] in the context of "optical rouge wave" generation in fibers, which represent Raman-shifting solitons with statistically rare high peak

#93705 - $15.00 USD Received 12 Mar 2008; revised 9 Apr 2008; accepted 9 Apr 2008; published 11 Apr 2008

amplitudes appearing as a result of soliton fission seeded by the modulation instability (MI).

In the context of SC generation using short pump pulses in the vicinity of zero dispersion (ZD), or slightly on the anomalous side, two important mechanisms contribute to the initial spectral broadening. When pumping with short pulses, such that $N \leq 10$, where N is a soliton number [14], the soliton compression, which occurs over several nonlinear lengths, supplemented by the emission of Cherenkov radiation at the phase-matched wavelengths across the ZD point are responsible for SC generation. Importantly, subsequent propagation after the initial pulse breakup does not lead to further substantial spectral extension, except for the slow Raman shift of solitons towards the red, which may add at best a few hundreds of nanometers to the overall SC width. In the case of longer pump pulses, $N \gg 10$, it is the MI that leads to formation of ultrashort solitons, their compression and Cherenkov emission [15]. In either case, the soliton fission is central to the SC generation mechanisms, and thus our detailed comprehension of the soliton fission, and its sensitivity to input pump pulse parameters, is paramount.

According to current understanding two noise sources may contribute to coherence degradation of the SC. Technical noise on the input pulse (e.g. energy, central wavelength, chirp, etc.) or coupling instabilities (e.g. pointing, fiber tip heating and vibration) propagate through the process of SC generation with mild amplification [4, 7] and with current pump laser technology play only minor role. In contrast, the fundamental quantum noise serves as a seed for MI and is amplified exponentially with the input pulse peak power [5]. Previous studies have shown that there exists a threshold at $N \sim 10$ beyond which incoherent MI seeded by quantum noise governs the generated SC properties [15]. On the anomalous dispersion side of the SC spectrum the noise characteristics are directly related to the shot-to-shot differences in the dynamics of solitons, manifested in their temporal jitter [16, 17].

It was recently recognized using numerical modeling [13] that the presence of low-frequency modulations on the pump pulse envelope may dramatically affect the soliton fission at the initial stage of SC evolution. In particular, it was shown that the frequency of occurrence of the rouge solitons can be controlled. However, no experimental results on SC generation with modulated pump pulse envelopes are available.

In this work we report on experimental analysis of SC generation using pulse shape-modulated femtosecond pump pulses. Slight modulations of the pump pulse envelope may be present at the output of certain types of laser systems, such as synchronously-pumped optical parametric oscillators in the vicinity of the degeneracy point, and comprise a type of technical noise, which looks more like the quantum noise, however, in the way it propagates through and affects the soliton fission and thus the overall SC generation. Similar to quantum noise these ripples serve as the seed for the MI and thus may lower the threshold value of N after which the generated SC becomes incoherent. The statistics of this noise, which may be highly non-Gaussian, is strongly amplified and propagated to the resulting SC, allowing easy experimental identification of the noise source. Because the soliton fission process is tremendously sensitive to the input pulse shape, we observe the effects of this type of noise through measurements of soliton timing jitter.

Direct experimental characterization of soliton timing jitter requires temporal resolution. Both auto-correlation and cross-correlation techniques can be used for time-resolved measurements of solitons [16–24]. In this work we apply the XFROG and FROG techniques to obtain spectrograms of the SC generated in the soft glass SF6 photonic crystal fiber (PCF) [25] with temporal and spectral resolution simultaneously. We compare our data to numerical results produced by integration of generalized nonlinear Schrodinger equation (GNLSE). From the experimental data the timing jitter of solitons can be directly observed. In addition, certain information on jitter statistics and the soliton behavior can be extracted and compared to separate measurements using a fast photodiode in a spectrally-resolved setup.

#93705 - $15.00 USD Received 12 Mar 2008; revised 9 Apr 2008; accepted 9 Apr 2008; published 11 Apr 2008

2. Experiment and modeling

Very few reports exist where the whole supercontinuum is visualized with simultaneous spectral-temporal resolution [20–22]. The obvious complication here is the need for the measurement system to be broadband enough to accommodate the octave- or more spanning SC spectra. Obviously, the required bandwidth of an autocorrelation-type system, such as FROG is approximately twice the SC bandwidth, while for a cross-correlation type measurement this requirement is substantially relaxed, because the reference pulse can be narrow-band, typically a portion of the pump pulse split off before the fiber and appropriately delayed. This is why all previous SC measurements relied on cross-correlation type approach. In [20, 21] a sum-frequency generation (SFG) XFROG technique was used with pump (and reference) pulses centered at 800 nm, the wavelength region where the material dispersion in the nonlinear SFG crystals precludes wide phase-matching (PM) bandwidths, so that complicated methods for PM extension, such as angular crystal dithering, were required. An alternative sonogram approach was employed in [22]. This method requires scanning both the delay and a tunable spectral filter, although clever solutions were offered.

In this work we used SFG-XFROG technique [26] to measure spectrograms of broadband SC generated in a SF6 PCF, pumped with 100 fs pulses at 1550 nm. In this wavelength range, broad PM bandwidths are possible in relatively thick BBO crystals, Fig.1, making it unnecessary to angle-dither the crystal. Among the three possibilities illustrated in Fig. 1, the Type 1 PM process $o_{sig} + o_{ref} \rightarrow e_{SF}$, where *o* and *e* denote the ordinary and extraordinary rays respectively and subscripts *sig*, *ref* and *SF* stand for "signal", "reference" and "Sum Frequency", is the most optimal for measurements of broadband SC centered around the pump wavelength of 1550 nm. Other signal wavelength regions may be accessed using the two Type 2 PM processes as illustrated in Fig. 1

In addition to XFROG other techniques were employed in our experiments. A typical scanning FROG system was used to gain information on the solitons' true duration and jittering statistics. Spectral measurements up to 2.5 μm were taken with a scanning FTIR spectrometer (Oriel, Mir 8000) equipped with an extended InGaAs photodiode detector. Laser spectrum was measured with high-dynamic range optical spectrum analyzer (ANDO AQ-6315E). Finally, the wavelength-dependent shot-to-shot behavior of the generated SC was measured in a spectrally-resolved setup consisting of a diffraction grating and a fast ($\approx$1 GHz bandwidth) photodiode connected to a digital phosphor oscilloscope (Tektronix TDS5052B).

The fiber used in the experiments was fabricated using the extrusion and drawing method from the Schott SF6 glass, which is characterized by $\sim$10 times higher intrinsic nonlinearity $n_2 = 2.2 \cdot 10^{-15}$ cm^2/W as compared to silica, and somewhat narrower transmission window [25]. The size of the guiding core was ~ 2.6 μm shifting the ZD point to $\approx$ 1300 nm so that the pump pulses are located in the anomalous dispersion region. At the pump wavelength of 1550 nm the dispersion $D \approx 50$ ps/nm/km so that for a transform-limited 100 fs pump pulse the dispersion length at the pump wavelength is $L_D \approx 5$ cm. For the pump pulse energies used in our experiments the nonlinear length can be sub-millimeter so that the soliton number $N = \sqrt{L_D/L_{NL}} \leq 7$ for the input pulse peak powers up to 10 kW. We used a 11 cm long SF6 PCF sample in the experiments, the length sufficient to observe soliton formation and dynamics, yet short enough to alleviate the losses.

A Ti:Sapphire oscillator-pumped optical parametric oscillator system (Spectra Physics Millenia, Tsunami and Opal) running at 81 MHz was employed as a source of 100 fs pump pulses centered at 1550 nm.

For the numerical modeling we used a typical GNLSE [27] supplemented with experimentally measured and numerically computed (based on an SEM image of fiber crossection) dispersion parameters, spectral loss data [25] and an experimentally measured Raman line of the

#93705 - $15.00 USD Received 12 Mar 2008; revised 9 Apr 2008; accepted 9 Apr 2008; published 11 Apr 2008

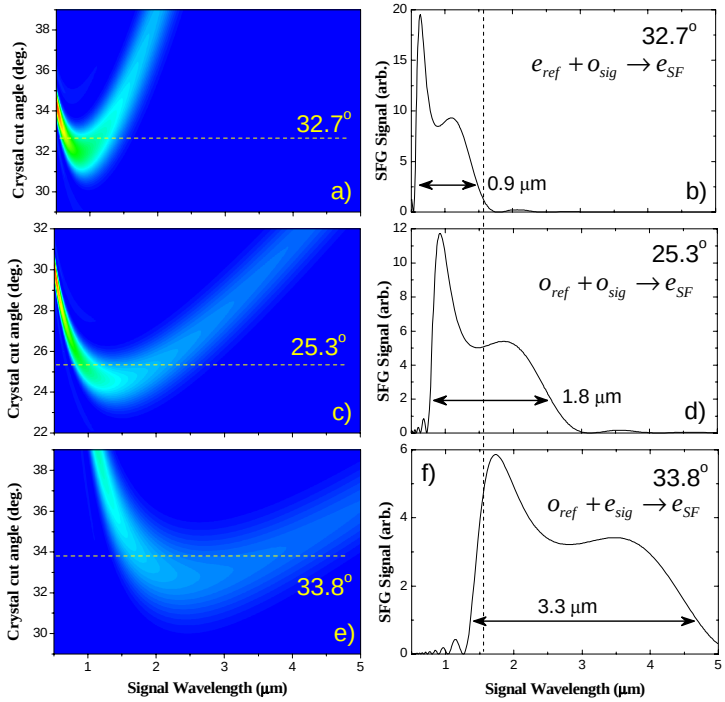

Fig. 1. Phase matching for non-collinear sum-frequency generation of fixed wavelength reference pulse at 1550 nm and variable wavelength signal pulse in a 200μm thick BBO crystal. Density plots are shown on the left for crystal cut angle vs. signal wavelength. Dashed lines show most optimal cut angles for obtaining large phase-matching bandwidths, and corresponding phase-matching curves are plotted on the right. (a) and (b): Type 2: $o_{sig} + e_{ref} \rightarrow e_{SF}$ SFG process; (c) and (d): Type 1: $o_{sig} + o_{ref} \rightarrow e_{SF}$ process; (d) and (f): Type 2: $o_{ref} + e_{sig} \rightarrow e_{SF}$ process. Vertical dashed line indicates $\lambda = 1.55$ μm central wavelength in our experiments.

fiber. The GNLSE was solved using the standard split-step method and the numerical XFROG traces were computed from the signal and reference pulses' complex electric fields.

3. Results and discussion

Figure 2 displays the numerical, Fig. 2(a), and experimental, Fig 2(b), XFROG spectrograms of the SC at the output of 11 cm long SF6 PCF for the soliton number $N \approx 4$. The input pulse energy is adjusted so that several solitons form on the anomalous dispersion side (longer wavelengths). It can be seen that a nearly two-octave PM bandwidth is achieved in the measurement, as suggested by Figs. 1(c) and (d).

The fact that the broadband radiation in general lies on the quasi-parabola, which corresponds to the group delay as a function of wavelength, suggests that all (or most) of the supercontinuum spectrum is generated at the very beginning of the fiber, supporting the previous findings [28]. Remarkably, the numerical model reproduces the experimental data very well. On the normal dispersion side (shorter wavelengths) the quasi-continuum is pierced with holes directly opposite to solitons [27]. As was predicted [27] and demonstrated in separate experiments [29, 30], the four-wave mixing (FWM) interaction of solitons and continuous waves

#93705 - $15.00 USD Received 12 Mar 2008; revised 9 Apr 2008; accepted 9 Apr 2008; published 11 Apr 2008

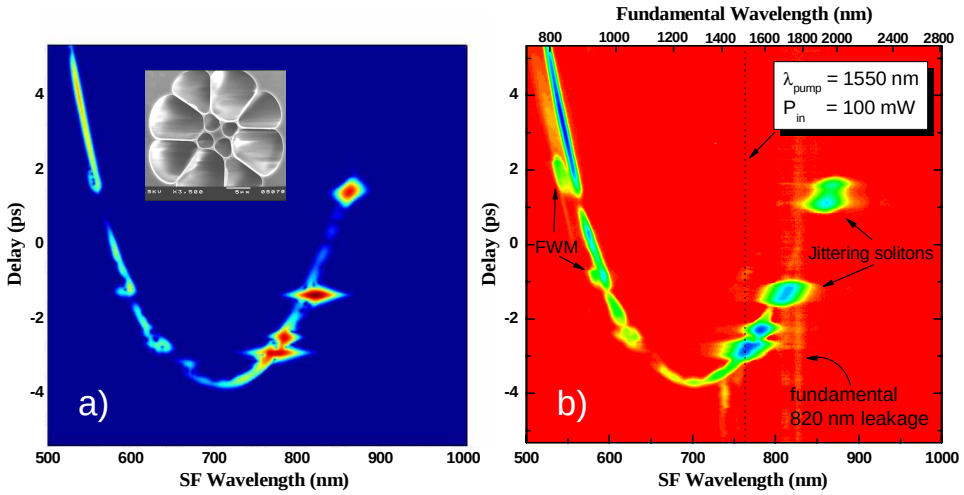

Fig. 2. Numerical, (a), and experimental, (b), XFROG spectrograms of a supercontinuum pulse at the output of 11 cm long piece of SF6 PCF pumped with 100 fs pulses at 1550 nm. Lower axis is sum-frequency and upper axis in (b) is fundamental wavelength of the signal. Color scale is logarithmic covering 30 dB of sum-frequency signal intensity. Inset shows the SEM image of the fiber tip.

leads to phase-matched emission of spectral components with wavelengths determined by the so-called ”phase-insensitive” scattering resonance [29].

This soliton-cw scattering is observed here in the process of SC evolution and the new spectral components are marked as ”FWM” in Fig. 2(b). Similar features were observed previously in experiments with highly nonlinear regular fiber [22] and were termed ”trapped components”. The fact that ”FWM” or ”trapped components” appear in this case on the outside of the group-delay parabola is related to the Raman self-frequency shift of the solitons towards longer wavelengths, i.e. also outside the ”parabola”. If, on the other hand, the SC generation was studied in the vicinity of the second ZD of a (perhaps different) fiber [31], the solitons would be driven by the Raman effect towards inside the ”parabola” and similarly the new FWM components would also be emitted inside the ”parabola”, in accordance with phase-insensitive resonance in soliton-cw scattering [27]. Additional insight into this effect can also be found in [32].

Important for us here, is the observation of temporal elongation of the solitonic components on the red side of the spectrum, marked “jittering solitons” in Fig. 2(b). The numerical results show no such elongation, with the exception of the red-most soliton, which is due to the intentional introduction of excessive confinement loss at longer wavelengths [25]. Still, the shape of the numeric XFROG trace for this soliton differs substantially from the experimental one. There could be three explanations for the observed elongation of the solitonic XFROG components: (1) the true temporal stretching of the pulses, (2) ejection of solitonic pairs [33], or (3) timing jitter of solitons on a shot-to-shot basis. Subsequent analysis proves the latter case of soliton timing jitter to be the cause of the observed dynamics.

To confirm unambiguously the presence of jitter and the absence of temporal elongation of the solitons themselves or soliton pair ejection we performed a separate set of measurements using FROG, Fig. 3. Being an autocorrelation-type measurement, FROG displays true pulse duration in the vicinity of zero delay, independent of any jitter present inside the complex pulse. Additionally, a soliton pair would result in a triple-peaked trace near zero delay, as in [33]. In our case, at least two red-most solitons are well isolated both spectrally and temporally, which

#93705 - $15.00 USD Received 12 Mar 2008; revised 9 Apr 2008; accepted 9 Apr 2008; published 11 Apr 2008

allows distinct FROG traces for those solitons near zero delay. Indeed, we see that for both low, Fig. 3(a) and high, Fig 3(b) input powers the zero-delay FROG traces at longer wavelengths comprise single and short (sub-100 fs) peaks. At the same time, the cross-correlation traces produced by the two red-most solitons in Fig. 3(b) appear temporally stretched, revealing the presence of relative timing jitter between individual solitons. The high degree of symmetry with respect to $t = 0$ in these FROG traces, as well as high reproducibility of these traces, rule out any slow drift in experimental conditions as the reason for the observed smear in cross-soliton correlation peaks. The observed jitter is a true shot-to-shot variability in the soliton temporal positions.

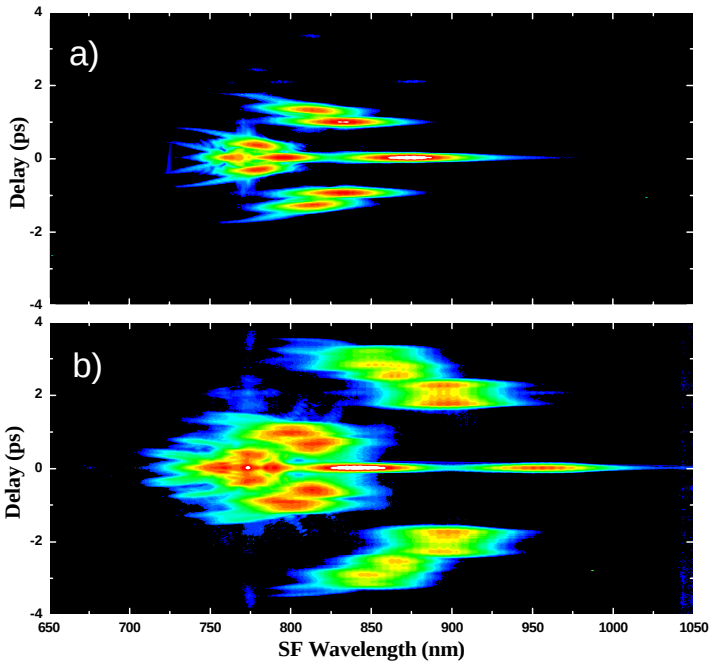

Fig. 3. Experimental FROG traces taken at the output of the same SF6 PCF sample as in Fig. 2 for "low" input average power of 40 mW (a) and "high" power of 100 mW (b). The blue portion of the SC was removed with a silicon filter so that only solitonic part of SC is shown. Color scale is logarithmic spanning 30 dB of sum-frequency signal intensity.

The results of FROG measurements in Fig. 3 suggest that the amount of soliton timing jitter depends strongly on the input power. This observation is verified directly in Fig. 4, where several XFROG traces of the solitonic part of the SC were taken for different input powers. Substantial jitter is observed only at the onset of formation of three solitons at ~ 80 mW input average power ($N \approx 3$) and above.

It can be inferred from Figs. 2–4, that the statistics of the temporal delays of the first (red-most) and second solitons are highly non-Gaussian. This is suggested by the shapes of the solitonic components on the XFROG traces of Figs. 2, and 4, and the cross-solitonic peaks on the FROG traces in Fig. 3(b). Specifically, it appears that solitons tend to occupy a certain delay range with near-uniform or even double-peaked, rather that Gaussian, probability distribution. These results are highly reproducible with exact same statistics and only slight variations in the extent of temporal jitter, which may be related to fiber coupling variations from experiment to experiment. The non-Gaussian nature of the statistics observed suggests technical noise as the

#93705 - $15.00 USD Received 12 Mar 2008; revised 9 Apr 2008; accepted 9 Apr 2008; published 11 Apr 2008

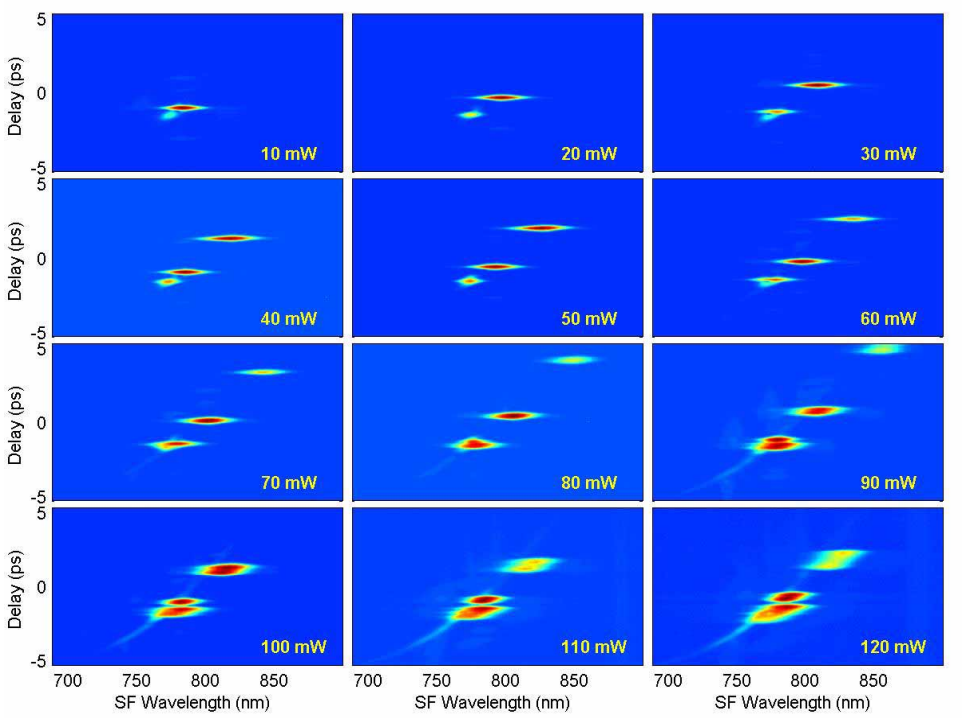

Fig. 4. Sequence of experimental XFROG spectrograms at the output of SF6 PCF, as in Fig. 2. Only solitonic part of SC shown. Multiple soliton formation is observed. Soliton timing jitter onset at 80 mW. Color scale is logarithmic. Horizontal axis is sum-frequency wavelength of the upconverted signal. For each panel the average input power is indicated, not adjusted for ∼30% coupling efficiency.

cause of the jitter.

Figure 3(b) also shows anticorrelation behavior of jittering solitons: if on one laser shot the first soliton moves to a longer wavelength, the second soliton tends to move to a shorter wavelength and vice versa. This behavior can be inferred from the shape of the cross-soliton peaks on the FROG traces of Fig. 3(b). Specifically, it can be seen that the central wavelength of the cross-soliton peak is delay-independent. Since delay is related to the central wavelength of the soliton we can naturally conclude that to produce a signal at larger or smaller delay *and* at the same sum-frequency the two solitons need to move in opposite directions on the wavelength axis from shot to shot.

Our extensive modeling using GNLSE shows that the extent of jitter observed in our experiments cannot be explained by realistic fluctuations in input pulse energy, spectral width or central wavelength. On the other hand, a particular source of input noise, namely the small-scale modulations of the input pulse envelope, explains well both the extent of the jitter observed and the anticorrelation behavior of solitons. Figure 5 illustrates the influence of the input pulse shape modulations on the soliton dynamics in the process of SC generation. Two slightly different pump pulse shapes are considered: The red curves correspond to the smooth input pulse, while the black curves correspond to the input pulse with a modulated envelope. To model the latter case we put two sidelobes on the pulse spectrum with peak intensities about 30 dB below the main peak. The addition of these sidelobes changes the input pulse energy by only

#93705 - $15.00 USD Received 12 Mar 2008; revised 9 Apr 2008; accepted 9 Apr 2008; published 11 Apr 2008

∼0.1%. From Fig. 5(a) we see that the soliton delays vary significantly between the smooth and rippled pump pulse cases. More importantly, however, Figs. 5(a) and 5(c) clearly show the presence of the anticorrelation in the temporal and spectral positions of the first and the second solitons, exactly as was observed in the experiments. It is intriguing to see that very small modulations of the pump pulse envelope affect the soliton fission process so dramatically, reinforcing the previously demonstrated ability to control the dynamics of soliton with shaped input pump pulses [34]. The spectral evolution of the SC generated with rippled pump pulses is also understandably different, Fig. 5(c), indicating that envelope-modulated pulses can be used to manipulate the spectral intensity of supercontinua.

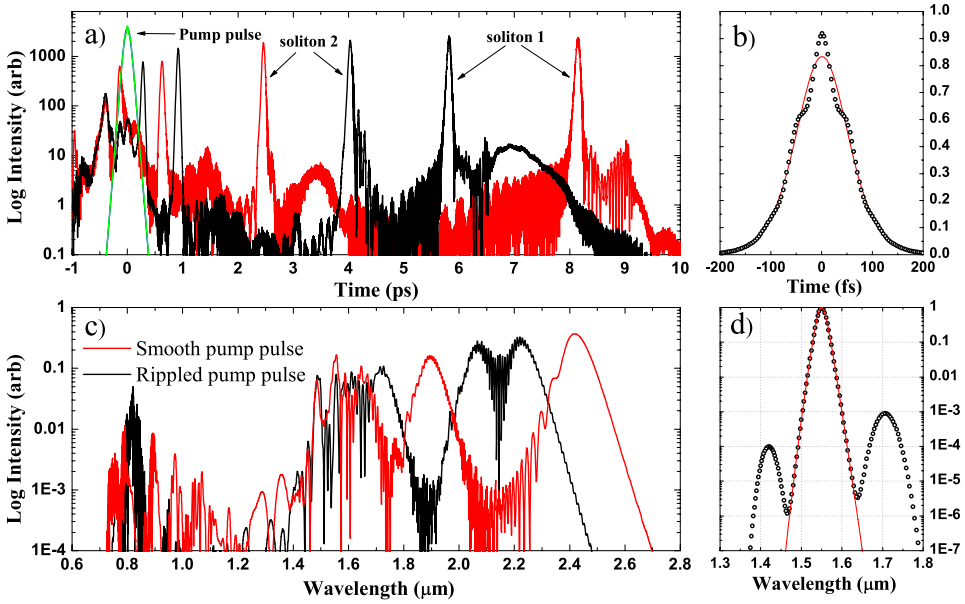

Fig. 5. Modeling results for the SC generated with smooth (red curves) and rippled (black curves) pump pulses in SF6 PCF used in the experiments: (a) temporal intensity at the PCF output; (b) details of the temporal envelope of the pump pulses; (c) spectral intensity at the output; (d) details of spectral content of the input pulses.

It appears that synchronously-pumped optical parametric oscillators, such as Opal, tuned near the degeneracy point display this particular type of noise, which affects the outcome of highly nonlinear experiments, such as SC generation, as shown here, or high-order soliton dynamics [34]. Figure 6 displays the Opal output spectrum tuned to 1550 nm with high dynamic range. Indeed, the Opal spectrum shows noticeable sidelobes around 1450 and 1650 nm. Moreover, the substantial noise present on these sidelobes indicates large fluctuations of the amplitude and/or the wavelength of these spectral components. The presence of the noise was directly verified by spectrally resolving the Opal output with a diffraction grating and using a fast photodiode to acquire the pulse train at a specific wavelength. The insets to Fig. 6 show the photodiode signals at the center wavelength and at the 1450 nm sidelobe. Clearly the latter displays almost 100% noise, while the 1550 nm signal is stable. Additionally, as can be inferred from the color density of the accumulated multi-shot photodiode traces the signal amplitude shows non-Gaussian double-peak distribution. Thus, it is concluded that the fluctuating sidelobes on the input pump spectrum result in modulations on the pulse envelope, which seed

#93705 - $15.00 USD Received 12 Mar 2008; revised 9 Apr 2008; accepted 9 Apr 2008; published 11 Apr 2008

the MI and severely affect the soliton fission process leading to SC coherence degradation and large timing jitter of solitons at the output of the PCF.

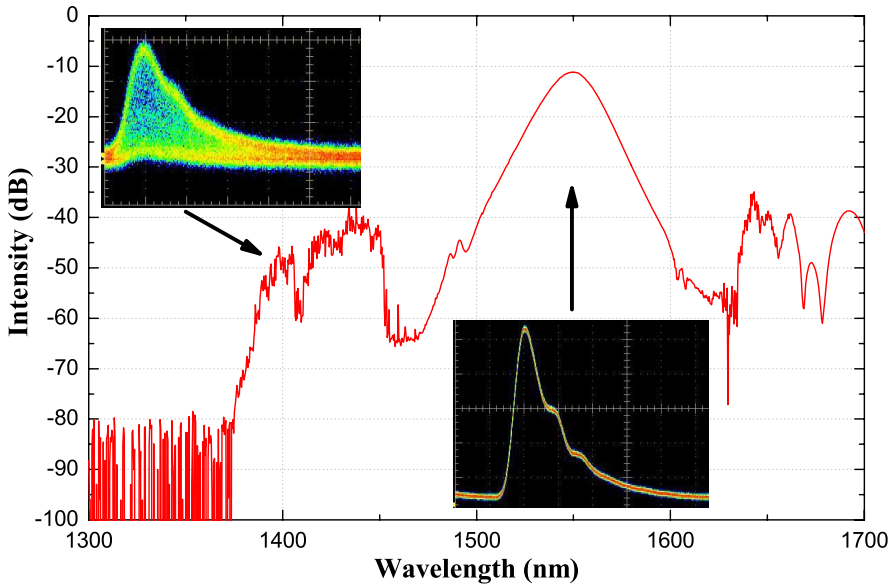

Fig. 6. Spectrum of the Opal system measured with high dynamic range. Noisy sidelobes are present on both sides of the main spectrum at $\sim 10^{-3}$ level. Insets show spectrally-resolved photodiode signals at the sidelobe and at the central wavelength. Warmer colors correspond to increased occurrences.

In a similar manner, a wavelength-dependent shot-to-shot noise of the SC can be measured using the same spectrally-resolved setup. Figure 7 shows the anomalous dispersion part of the SC spectrum in the regime of large jitter ($N \approx 4$). The insets show the accumulated photodiode signals at two wavelengths corresponding to the wings of the two red-most solitons. We clearly observe a large degree of noise corresponding to solitons jumping around in wavelength. As before, the color density of the plots convey non-Gaussian double-peaked probability distribution, comparable to that present on the pump pulse spectrum wings.

The sensitivity of the soliton fission process to the presence of ripples on the input pulse envelope has been studied in the past; however, the soliton anticorrelation behavior has not been noticed. For this type of noise to be important in the experiments the frequencies of the ripples must fall near the peak of the MI gain, $\Omega_{max} = \sqrt{2\gamma P_0/|\beta_2|}$, where γ is the effective nonlinearity of the fiber, P_0 is the peak power of the pump pulse and β_2 is the dispersion at the pump wavelength [14]. For the fiber parameters used in our experiments this corresponds to the ripples with periods of about 20-100 fs for the peak powers in the neighborhood of 1 kW, similar to Fig. 5. Therefore, the ripples of this temporal scale will experience the largest MI gain and will outgrow any other noise present on the pulse, such as the broadband quantum noise. It is clear, therefore, that, as compared to quantum noise, the pulse shape noise lowers the threshold in N beyond which the SC displays substantial coherence degradation.

The existence of the threshold in N, or pump power, for the onset of the substantial jitter and coherence degradation is easy to understand by comparing the relative efficiencies of MI and regular deterministic soliton fission of a smooth pulse. To this end we introduce a pair of characteristic lengths describing these processes. For the deterministic soliton fission the

#93705 - $15.00 USD Received 12 Mar 2008; revised 9 Apr 2008; accepted 9 Apr 2008; published 11 Apr 2008

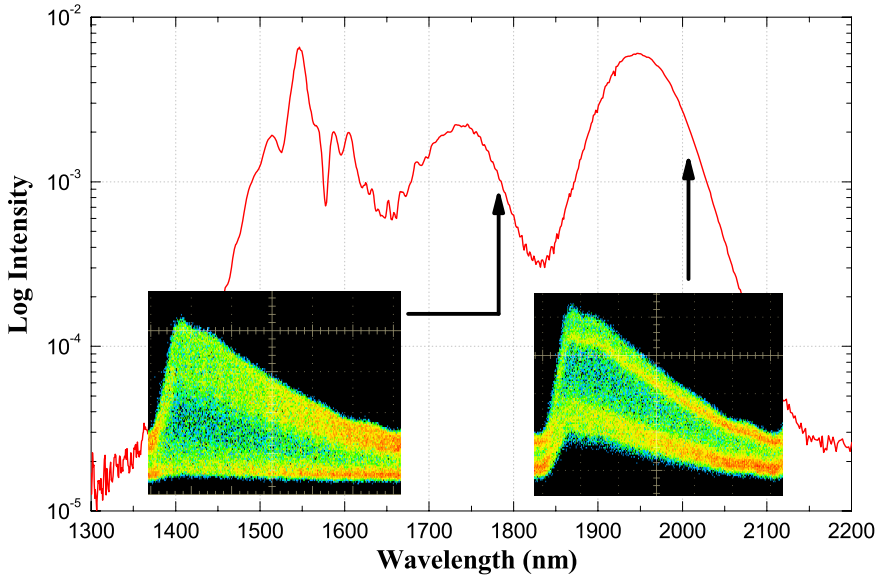

Fig. 7. Solitonic part of the SC spectrum. Two redmost solitons are clearly identifiable. Insets show spectrally-resolved photodiode signals at the wings of the soltions‘ spectra. Warmer colors correspond to increased occurrences.

empirical value of the characteristic length is $L_{fiss} \approx L_D/N$ [15], which is inversely proportional to the square root of the pump pulse power, whereas the characteristic length for the MI, $L_{MI} = 1/2\gamma P_0$, depends inversely on the power. Thus, with increasing the input pulse peak power P_0 the MI characteristic length will become shorter than L_{fiss} at the critical power P_0^{crit} given by $L_{fiss} = L_{MI}$, or

$$P_0^{crit} = \frac{|\beta_2|}{4\gamma T_0^2}, \tag{1}$$

where T_0 is the input pulse duration. This means that there is a threshold with respect to the input pump power after which the deterministic fission will be overcome by the MI-seeded fission thus changing the nature of the SC from coherent to incoherent. For our experimental conditions the estimated value for the critical power is $P_0^{crit} \approx 0.1$ kW, whereas the observed value is over 1 kW. This discrepancy is not surprising, however, given the crudness of the analysis and the uncertainty in the actual amplitude of the ripples present on the input pulse. Nevertheless, this analysis explains the presence of the threshold in the SC generation where the coherence properties of the SC change abruptly, as observed in our experiments.

4. Conclusion

In this work we investigated the supercontinuum generation in a soft glass SF6 photonic crystal fiber pumped with envelop-modulated 100 fs pulses. XFROG measurements reveal the details of the SC dynamics, interaction of solitons with quasi-continuous waves across the zero-dispersion wavelength and generation of phase-matched ”FWM” or ”trapped components”. At higher input powers we observe the onset of severe timing jitter of solitons on the anomalous side of the SC. Subsequent FROG measurements confirm the presence of jitter and also reveal the anticorrelation behavior of the two red-most solitons in which the solitons tend to move

#93705 - $15.00 USD Received 12 Mar 2008; revised 9 Apr 2008; accepted 9 Apr 2008; published 11 Apr 2008

in opposite directions on the time and wavelength axes from shot to shot. The observed jitter results from the presence of a slight modulation riding on top of the pump pulse temporal envelope. Numerical modeling supports this conclusion. The ripples effectively seed the modulation instability and strongly affect the soliton fission. Analysis shows that the MI overwhelms the deterministic soliton fission at a certain threshold power, which is lower than the expected value for quantum-noise seed. The input pulse envelope modulations are thus identified as an additional source of technical noise, which may be important in experiments. The envelope modulation frequencies produced by our laser system are comparable to the ones deemed optimal for control of optical rouge waves [13] and can potentially be used in future experimental demonstration of optical rouge wave control.

Acknowledgements

This work was performed, in part, at the Center for Integrated Nanotechnologies, a U.S. Department of Energy, Office of Basic Energy Sciences user facility. Los Alamos National Laboratory, an affirmative action equal opportunity employer, is operated by Los Alamos National Security, LLC, for the National Nuclear Security Administration of the U.S. Department of Energy under contract DE-AC52-06NA25396. The authors gratefully acknowledge Jonathan C. Knight and his group at the Centre for Photonics and Photonic Materials, Department of Physics, University of Bath, UK for providing the samples of SF6 PCFs and for numerous fruitful discussions.

#93705 - $15.00 USD Received 12 Mar 2008; revised 9 Apr 2008; accepted 9 Apr 2008; published 11 Apr 2008